Nanoscale Res Lett (2009) 4:1335–1342
DOI 10.1007/s11671-009-9402-y

NANO EXPRESS

Controlled Growth of WO_3 Nanostructures with Three Different Morphologies and Their Structural, Optical, and Photodecomposition Studies

S. Rajagopal · D. Nataraj · D. Mangalaraj · Yahia Djaoued · Jacques Robichaud · O. Yu. Khyzhun

Received: 2 June 2009 / Accepted: 17 July 2009 / Published online: 4 August 2009

Abstract Tungsten trioxide (WO_3) nanostructures were synthesized by hydrothermal method using sodium tungstate ($Na_2WO_4{\cdot}2H_2O$) alone as starting material, and sodium tungstate in presence of ferrous ammonium sulfate [$(NH_4)_2Fe(SO_4)_2{\cdot}6H_2O$] or cobalt chloride ($CoCl_2{\cdot}6H_2O$) as structure-directing agents. Orthorhombic WO_3 having a rectangular slab-like morphology was obtained when $Na_2WO_4{\cdot}2H_2O$ was used alone. When ferrous ammonium sulfate and cobalt chloride were added to sodium tungstate, hexagonal WO_3 nanowire clusters and hexagonal WO_3 nanorods were obtained, respectively. The crystal structure and orientation of the synthesized products were studied by X-ray diffraction (XRD), micro-Raman spectroscopy, and high-resolution transmission electron microscopy (HRTEM), and their chemical composition was analyzed by X-ray photoelectron spectroscopy (XPS). The optical properties of the synthesized products were verified by UV–Vis and photoluminescence studies. A photodegradation study on Procion Red MX 5B was also carried out, showing that the hexagonal WO_3 nanowire clusters had the highest photodegradation efficiency.

Keywords Tungsten trioxide · Hydrothermal · Structure-directing chemicals · Nanowires · Nanorods · Photodecomposition

S. Rajagopal · D. Nataraj (✉)
Thin Film & Nanomaterials Laboratory, Department of Physics, Bharathiar University, Coimbatore 641 046, India
e-mail: de.natraj@gmail.com

D. Mangalaraj
Department of Nanoscience and Technology, Bharathiar University, Coimbatore 641 046, India

Y. Djaoued · J. Robichaud
Laboratoire de Micro-Spectroscopies Raman et FTIR, Université de Moncton-Campus de Shippagan, 218, boul. J.-D. Gauthier, Shippagan, NB E8S 1P6, Canada

O. Yu. Khyzhun
Department of Structural Chemistry of Solids, Frantsevych Institute for Problems of Materials Science, National Academy of Sciences of Ukraine, 3 Krzhyzhanivsky Street, 03142 Kyiv, Ukraine

Introduction

One-dimensional (1-D) nanostructures have attracted much attention because of their distinct properties and wider applications. Self-assembled growth of one-dimensional nanostructures is a simple and spontaneous process. However, understanding the reaction chemistry and growth mechanism of the process is necessary to obtain these structures. Repeated experiments of this synthetic method are needed to obtain uniform growth of 1-D nanostructures.

Semiconductor metal oxide nanostructures are highly attractive, so more attention has been paid, because of their obvious optical and electronic applications. Tungsten trioxide (WO_3) is one of the *n* type indirect wide band gap materials [1, 2]. It is a fundamental functional material having interesting physical properties and wide range of applications. Due to its high work function, it was used as a charge injection layer [3]. Because of its higher catalytic activity, it can be used in photocatalytic and electrocatalytic applications [4, 5]. It serves as a good host for ions, so it can be used successfully in electrochemical Li ion batteries, electrochromic, thermochromic, and photochromic devices [6–9]. Many methods have been developed to synthesize 1-D WO_3 nanostructures, such as template-assisted growth [4], anodization [10], conventional thermal evaporation [1], hot wall chemical vapor deposition [11],

arc discharge [12], pulsed laser deposition [13], and hydrothermal method [14]. Among the various methods, hydrothermal method is a facile, dominant tool for the synthesis of anisotropic nanoscale materials. Significant advantages of this method are controllable size, low temperature growth, cost-effectiveness, and less complicated. Number of attempts were paid to synthesize controlled WO_3 nanostructures by hydrothermal method with the help of structure-directing chemicals like Na_2SO_4, Rb_2SO_4, K_2SO_4, Li_2SO_4, and Na_2S [6, 14–17]. All attempts suggest that the reason behind the controlled growth was due to the presence of sulfate ions in the reaction. The data reported in Refs. [6, 14–17] show that I-group compounds such as Li_2SO_4, Na_2SO_4, Na_2S, K_2SO_4, and Rb_2SO_4 were used as structure-directing chemicals for the synthesis of WO_3 nanostructures. In the present work, we choose VIII-group metal complexes, such as ferrous ammonium sulfate, as structure-directing chemical for the synthesis of WO_3 nanostructures. Since chlorine is next to sulfur in periodic table, we expect that it may have similar tendency to sulfur. Therefore, cobalt chloride was also used as another structure-directing chemical to realize the change in morphology of WO_3 products. It is interesting that we have obtained wire- and rod-shaped WO_3 nanostructures, respectively, from ferrous ammonium sulfate and cobalt chloride as structure-directing agents. Their structural, optical, and photodegradation properties were also studied in this paper.

Experimental Details

Synthesis of Tungsten Oxide Nanostructures

All the chemicals were of analytical grade and taken without further purification or modification. Sodium tungstate ($Na_2WO_4{\cdot}2H_2O$) is the starting material. Hydrochloric acid (HCl), oxalic acid ($C_2H_2O_4{\cdot}2H_2O$), nitric acid (HNO_3), ferrous ammonium sulfate [$(NH_4)_2Fe(SO_4)_2{\cdot}6H_2O$], and cobalt chloride ($CoCl_2{\cdot}6H_2O$) were the other chemicals used for the growth.

Three different reactions were made for the preparation of WO_3 products. In the first experiment, sodium tungstate was dissolved in 100 mL double distilled water (DDW) (6.6 g, 0.2 mole) and acidification was done by adding HCl to get a pH of 1. A white precipitate was obtained, and it was dissolved by adding oxalic acid (0.4 g in 30 mL DDW, 0.1 mole). As a result, a transparent solution was obtained, and it is the final solution for this experiment. In the second reaction, sodium tungstate (6.6 g, 0.2 mole) and ferrous ammonium sulfate (0.4 g, 0.1 mole, 10 mL DDW) were dissolved in DDW separately and mixed under vigorous stirring. A dark brown color mixture was obtained, and it was dissolved by adding oxalic acid. In this case, a transparent yellow color solution was obtained. It is the final solution of this reaction and its pH was 1. In the third experiment, sodium tungstate (6.6 g, 0.2 mole) and cobalt chloride (1.786 g, 0.5 mole, 15 mL in DDW) solutions were prepared separately and mixed with constant stirring. A violet mixture appeared, and it was dissolved by nitric acid. Now, a transparent red solution was obtained and its pH was 1. These three solutions were transferred separately into 40 mL Teflon-lined stainless steel autoclave and maintained at 180 °C for 24 h to get the final product. The as-obtained products were washed several times both in water and ethanol and finally dried at 100 °C for 2 h.

Characterization Techniques

The surface morphology, structural, and chemical states of the formed nanostructures were characterized by using scanning electron microscopy (SEM-5600 JEOL JSM), transmission electron microscopy (TEM-2011 JEOL STEM), X-ray diffraction (PANalytical X-ray diffractometer—XPERT PRO), Raman spectroscopy (Horiba Jobin Raman spectrometer, reflection mode, wavelength of 532 nm, 2mW), and X-ray photoelectron spectroscopy (XPS—ion-pumped chamber of an ES-2401 spectrometer Mg Kα radiation, photon energy 1,253.6 eV) techniques. Optical measurements were carried out in UV–Vis spectrophotometer (SHIMADZU 3600 UV–Vis–NIR spectrophotometer), and photoluminescence properties were analyzed by using Horiba Jobin Yvon spectrofluoromax spectrometer.

Results and Discussion

Characterization of Surface Morphology and Structural Properties

Figure 1a–c shows the scanning electron microscope (SEM) images of the as-prepared WO_3 products synthesized using three different hydrothermal reactions. Rectangular slab-like WO_3 crystals were obtained by direct hydrothermal synthesis. These rectangular slab-like structures show their sharp corners and smooth surfaces as indicated in the Fig. 1a. When ferrous ammonium sulfate was used, WO_3 nanowire clusters were obtained, and their SEM image is shown in Fig. 1b. The average length and diameter of the nanowires were 1 μm (1,000 nm) and 30 nm, respectively. Cobalt chloride-reacted WO_3 products, shown in Fig. 1c, look like rod-shaped nanostructures. Their average length and diameter were only about 100 and 30 nm, respectively. There is no change in the cross-sectional dimension between nanowires and nanorods, but

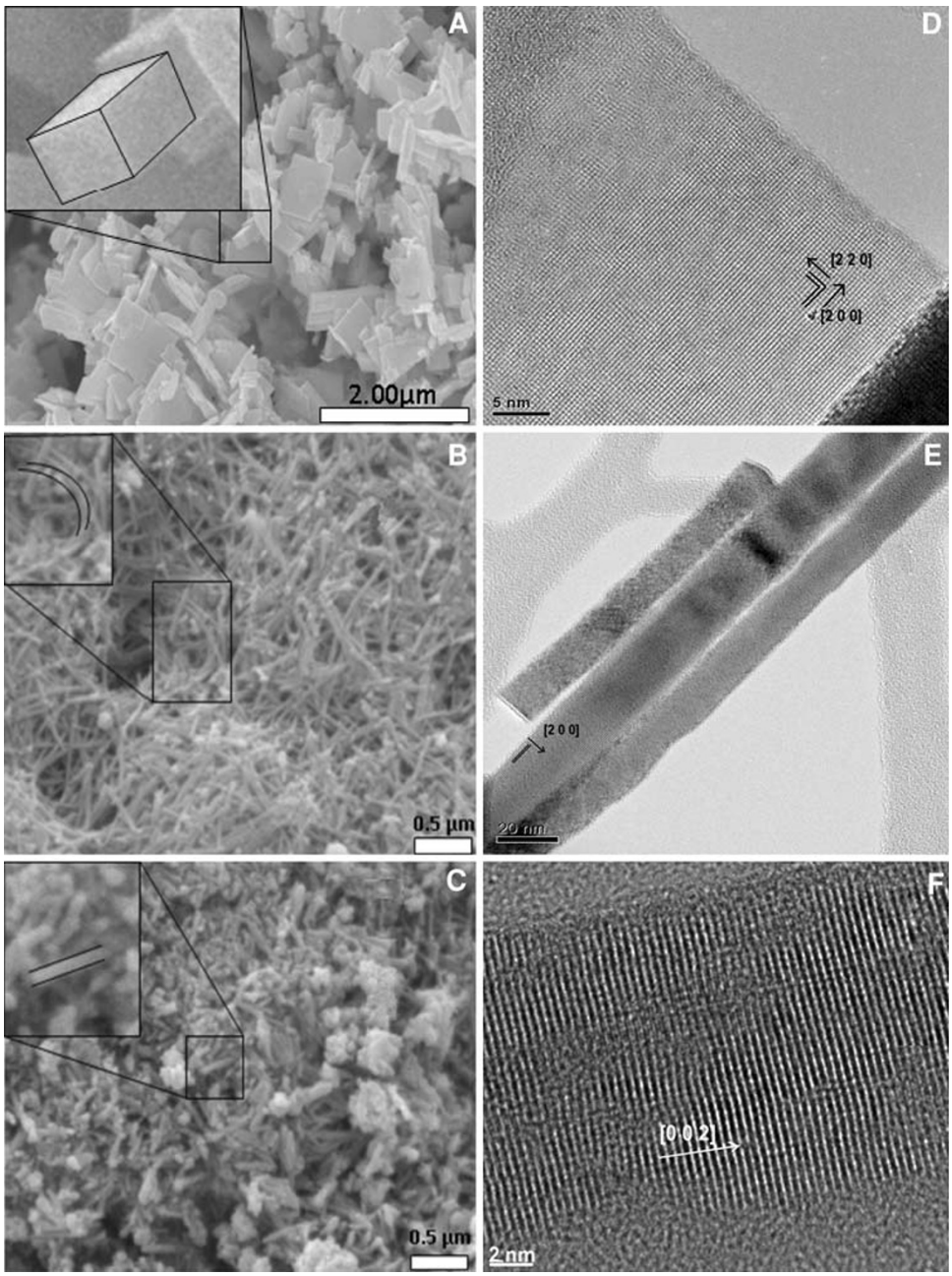

Fig. 1 SEM and TEM images of the three WO_3 morphologies: **a** and **d** rectangular slab, **b** and **e** nanowire clusters, and **c** and **f** rod-like structure

a decrease in the length was observed with nanorod morphology.

Usually, when there is no structure-directing chemical, the morphology will be rectangular in shape. When structure-directing chemicals such as sulfate and chlorine ions were added, then one can see the formation of one-dimensional nanowire/nanorod-like structures. Though the exact reason is not reported, it is believed that sulfate ions play a major role in giving one-dimensional shape, i.e., sulfate ions adsorb to the surface of the seed crystals of WO_3 and thereby decrease the surface energy of the WO_3 seed crystals in all directions except one direction. In this particular undisturbed direction, further growth takes place by means of agglomeration/attachment with other seed layers. This process continues to give one-dimensional wire/rod-like structures.

Figure 1d–f also shows that the corresponding high-resolution transmission electron microscope (HRTEM) images. Rectangular slab structures have shown well-cleared sharp boundaries. Resolved lattice fringes of both directions have been seen in rectangular slab structure. The calculated spacing of the lattice fringes of two perpendicular directions was about 3.14 and 3.63 Å, respectively. Figure 2a–c shows the X-ray diffraction (XRD) patterns for three as-prepared WO_3 products. XRD pattern for rectangular slab structure, with orthorhombic crystal phase,

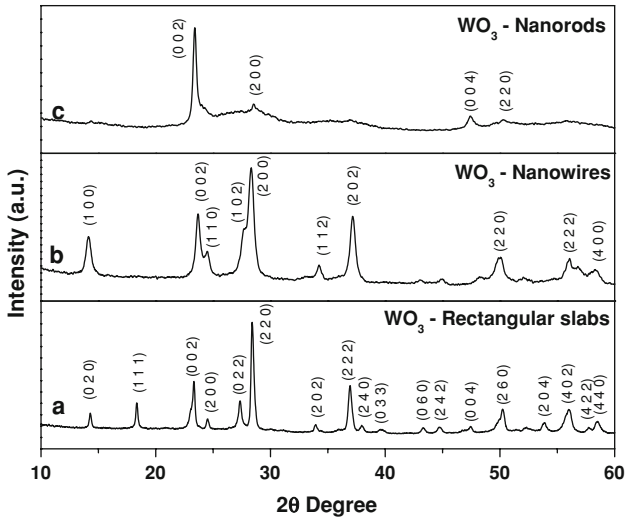

Fig. 2 X-ray diffraction spectra of the three different as-prepared WO_3 products: *a* rectangular slab-like structures, *b* nanowire clusters, and *c* rod-like samples

is shown in Fig. 2a. Spacing of the lattice fringes, calculated from the HRTEM, was well indexed with (220) and (200) planes of orthorhombic WO_3 crystals. Their lattice parameters were $a = 7.359$ Å, $b = 12.513$ Å, and $c = 7.704$ Å (JCPDS card No: 35-0270) [18]. HRTEM image of a nanowire shows (Fig. 1e) clear lattice fringes along the growth direction. Here, the spacing of the lattice fringes was 3.63 Å, which was well indexed with the 'd' spacing of the plane (200) of hexagonal WO_3 (Fig. 2b). These products were prepared by using ferrous ammonium sulfate as structure-directing chemical. They follow hexagonal crystal structure. Lattice parameters of the synthesized h-WO_3 are $a = 7.324$ Å and $c = 7.668$ Å (JCPDS card No: 85-2460) [14]. From the HRTEM image of WO_3 nanorod, it was observed that the spacing of lattice fringes was about 3.87 Å, which is indexed with the (002) plane in XRD pattern for the h-WO_3 products (Fig. 2c). These were prepared by using cobalt chloride as structure-directing chemical, and their lattice parameters are the same as that of WO_3 nanowire clusters.

Orthorhombic WO_3 structures are the usual product from the direct hydrothermal synthesis. However, when reacted with ferrous ammonium sulfate, it was observed that one of its lattice parameters '*b*' is reducing from 12.513 to 7.324 Å. The remaining lattice parameters '*a*' and '*c*' are almost unchanged in such a case. So, it is clear that the formation of hexagonal crystal structure from the orthorhombic structure is taking place by reducing '*b*' lattice significantly. The interlayer spacing for the direct synthesized WO_3 and ferrous ammonium sulfate used WO_3 products, respectively, at d220 (3.143 Å) and d200 (3.156 Å) are almost the same, which proves that the lattice parameters '*a*' and '*c*' are similar to each other. When reacted with cobalt chloride, a reduction in the '*b*' value close to '*a*' value was noted and that could be the reason for the change in crystal structure from orthorhombic to hexagonal. Though the exact reason behind the one-dimensional nanorod growth is not clear, we believe that chlorine ions also play a similar role as that of sulfate ions and help to grow a one-dimensional nanostructure.

In hydrothermal growth condition, nanoparticles of WO_3 are formed and subsequently aggregated to give morphologies like rectangular slab, wire, and rod structures. When there are no structure-directing chemicals, the as-formed nanoparticles are of orthorhombic nature and these orthorhombic nanoparticles aggregated to form a three-dimensional rectangular slab-like structure. When structure-directing chemicals, such as ferrous ammonium sulfate or cobalt chloride, were used, the as-formed WO_3 particles are of hexagonal nature and these hexagonal particles aggregated to give wire- or rod-like structures. Three-dimensional rectangular slabs-like structure is prohibited by the presence of sulfate or chlorine ions. The role played by the sulfate/chlorine ions in getting one-dimensional structure has been explained earlier.

Figure 3a–c shows the Raman spectra recorded from the three WO_3 samples. Most of the vibrational modes are similar to one another, but a very few modes differentiate whether it is orthorhombic or hexagonal WO_3 crystal system [19]. Crystalline WO_3 has three main spectral regions, one is between 900 and 600 cm^{-1}, the second one is between 400 and 200 cm^{-1}, and the third one is below 200 cm^{-1}. The three regions, respectively, correspond to stretching, bending, and lattice modes. These peaks are characteristics of tungsten oxide material as well. We observed Raman peaks for orthorhombic rectangular slab-like structure at 805, 690, 325, and 255 cm^{-1}. Here, the

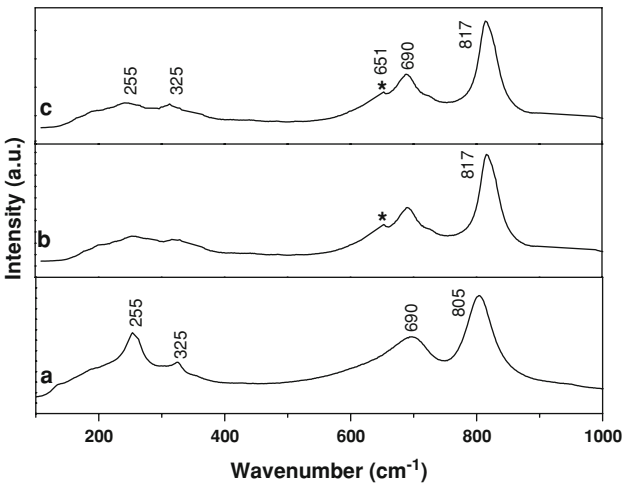

Fig. 3 Raman Spectra for WO_3 *a* rectangular slab, *b* nanowire clusters, and *c* nanorods samples

mode at 805 and 690 cm^{-1} corresponds to stretching vibration of O–W-O, whereas the modes at 325 and 255 cm^{-1} corresponds to bending vibration of W–O-W. In the case of the hexagonal nanowire structure, we observed almost similar modes as that of orthorhombic structure. The modes are 817 and 690 cm^{-1} and which were due to stretching vibrations. Upon comparing the stretching modes of orthorhombic (805 cm^{-1}) and hexagonal (817 cm^{-1}) structures, in the case of hexagonal WO_3, it was found that there is a shift in wavenumber toward higher side (Fig. 3b, c). This shift could be due to a local structural change in the crystal system, upon conversion from orthorhombic to hexagonal crystal structure. In addition to this, we also noticed a characteristic mode of hexagonal WO_3 at 651 cm^{-1} [20], which again confirmed the crystal structures of nanowire and nanorods. No impurity peaks other than WO_3 were observed, which shows the purity of the as-prepared samples.

Characterization of Chemical States

X-ray photoelectron spectroscopy (XPS) analysis was carried out to further confirm the purity of the samples and

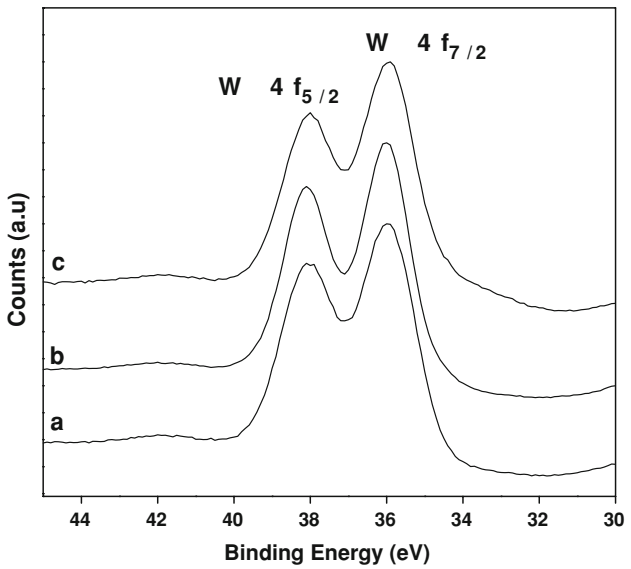

Fig. 4 XPS W 4f core-level spectra of as-prepared WO_3 products: *a* rectangular slab-like structures, *b* nanowire clusters, and *c* rod-like samples

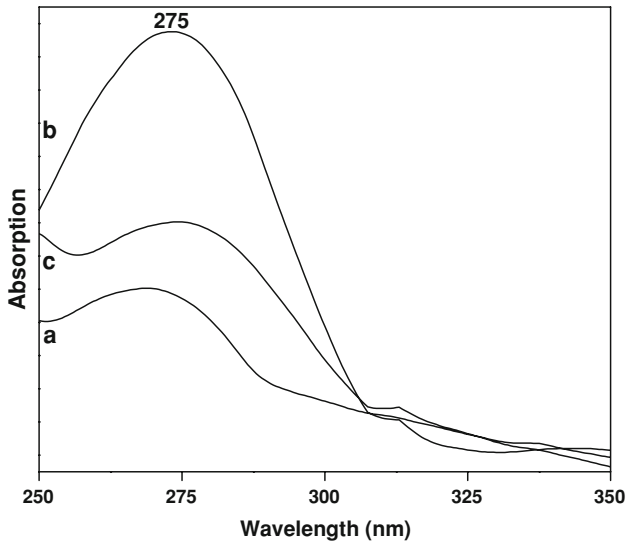

Fig. 6 UV–Vis absorption spectra of as-prepared WO_3 products: *a* rectangular slab-like structures, *b* nanowire clusters, and *c* rod-like samples

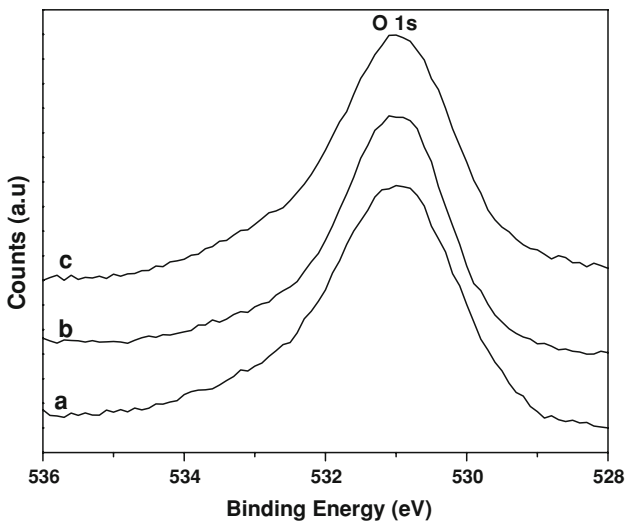

Fig. 5 XPS O 1s core-level spectra of as-prepared WO_3 products: *a* rectangular slab-like structures, *b* nanowire clusters, and *c* rod-like samples

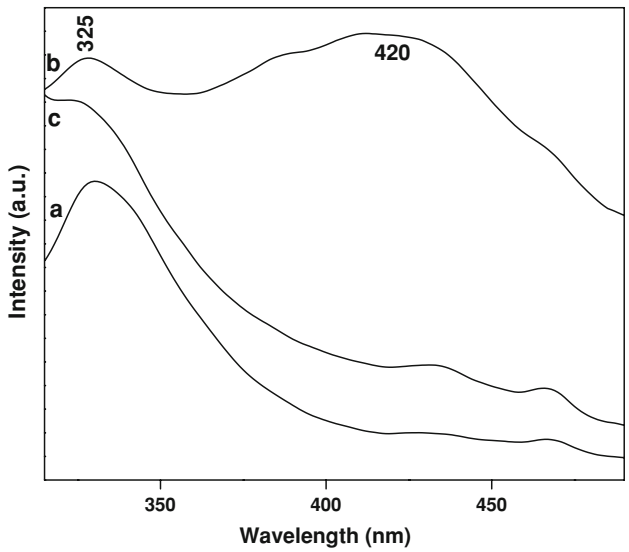

Fig. 7 Photoluminescence spectra of as-prepared WO_3 products: *a* rectangular slab, *b* nanowire clusters, and *c* rod-like samples

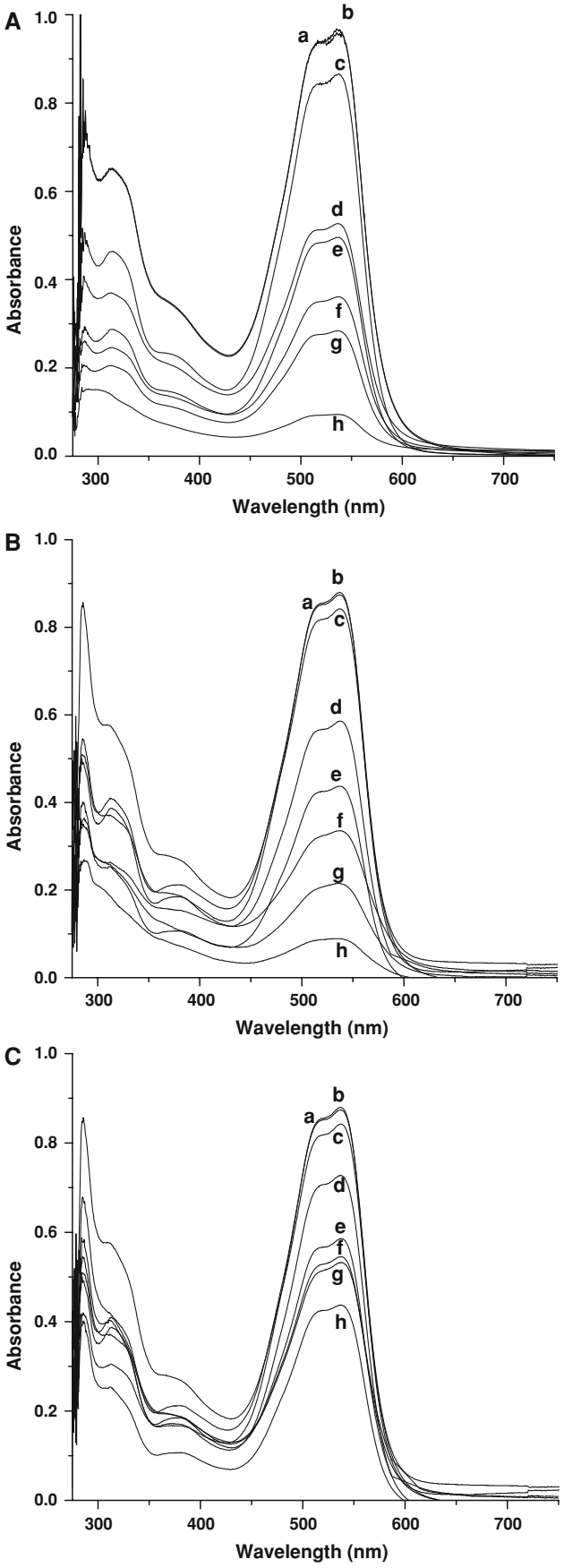

◀**Fig. 8** UV–Vis absorption spectral changes of Procion MX-5B dye mixed with WO_3 samples at different timings. **a** Rectangular slab WO_3 + Procion dye, **b** nanowire clusters WO_3 + Procion dye, and **c** rod-like WO_3 + Procion dye. Absorption spectra (*a*, *b*, and *c*), respectively, correspond to pure Procion MX-5B dye, Procion MX-5B dye in the dark for 24 h, and Procion MX-5B dye kept under UV illumination for 24 h, in the absence of WO_3 nanostructure. Spectra (*d*–*h*) corresponds to UV illumination time; 3, 6, 9, 12, and 24 h in the presence of WO_3 nanostructures

also to check the electronic state of the samples. Figure 4a–c shows the XPS W 4f core-level spectra for all the three as-prepared WO_3 samples. From these results, we observed that impurities like Fe, Co, Cl, N, and S are not present in all the three samples. The XPS W 4f core-level spectra have revealed that in all the samples under study tungsten atoms are in the formal valence state +6 [21]. Their 4f peaks binding energies were observed at 38.0 and 36.0 eV, which corresponds to spin-orbit splitting of the W $4f_{7/2}$ and W $4f_{5/2}$ components, respectively, in tungsten oxides [21]. The XPS O 1 s core-level binding energies of the tungsten oxide samples under consideration correspond to 531.0 eV (Fig. 5a–c). From the relative intensities of the XPS spectra, we have calculated the compositional stoichiometry between 'W' and 'O' and it is found to be about 1:3 in the every sample studied.

Characterization of Optical Properties

To study the photoluminescence as well as photodegradation performance of the as-prepared WO_3 samples, it is necessary to know the absorption edge and number of photons absorbed by the material. So, UV–Vis absorption spectra were taken for all the three WO_3 samples. Figure 6a–c shows the absorption spectra with a peak maximum at 275 nm wavelength for all the three samples. A very clear, high intense absorption peak was obtained for nanowire cluster structures, whereas for nanorod and rectangular slab structures less intense absorption was seen. Using this absorption maximum, photoluminescence property of the as-prepared WO_3 nanostructures was studied and their emission results are shown in Fig. 7a–c. We have seen emission peaks at 325 and 420 nm for all the three WO_3 samples. The emission at 325 nm corresponds to edge emission [22–25]. Only nanowire clusters have shown relatively high intense another emission peak at 420 nm and which could originate from the presence of oxygen vacancies or defect states [23]. Though XPS results have shown a stoichiometry in composition, our PL results have shown the presence of defect states by means of an emission at 420 nm. This could be due to more sensitivity of PL than XPS. Increase in surface to volume ratio results in increase of defect states in the case of WO_3 nanowire clusters and that could be the reason for the observed

strong visible emission in this sample. Rectangular slab and rod-shaped morphologies weakly exhibited this characteristic peak with noticeable intensity as shown in the Fig. 6a, c.

Photodecomposition Measurements

Photodecomposition activities of the as-prepared WO_3 nanostructures were analyzed with Procion Red MX-5B. We have chosen this dye for the decomposition purpose, because it is one of the harmful environmental pollutants. Attempts were made to decompose it by using TiO_2 nanoparticles in a typical photocatalytic reactor [26]. Since WO_3 nanostructures could also exhibit good photocatalytic performance, we used this for our photodecomposition study. For the present study, we used 0.25 mmole of Procion Red MX-5B reactive dye in 20 mL of DDW and about 0.05 g of all the three as-prepared WO_3 powders were mixed with the as-prepared dye solution and the photodecomposition experiment was carried out. A 2.0 mW UV light source with 365 nm wavelength was used for this work. Three experiments were carried out with three different WO_3 nanostructure morphologies. The absorption spectra changes during the photodecomposition of the reactive dye and resulted with a decrease in the absorption maximum. The results are shown in Fig. 8a–c for all the three morphologies. Absorption value a, b, and c in Fig. 8, respectively, correspond to pure as-prepared dye, dye in dark for 24 h, and dye kept in UV light for 24 h, but without WO_3 dispersion. From the observed results, we come to a conclusion that there is no any noticeable change when maintained for 24 h in dark, but a slight decrease in absorption was observed after 24 h exposure in UV illumination. With this initial study, the as-prepared WO_3 nanostructures were dispersed in the dye solution and illuminated with UV light for 3, 6, 9, 12, and 24 h and their absorptions were recorded. The spectra in Fig. 8d–h correspond to respective absorption spectra from the overall experimental results. Upon comparison of all the results, it was found that the WO_3 nanowire cluster dispersed medium has responded quickly in decomposing the dye. UV–Vis absorption spectra have shown that, only this particular morphology has high cross-section for absorption of photons, and this could be the reason for the quick response in decomposition.

To estimate the rate of the reaction in the present photodegradation experiment, the following equation was used:

$$\ln(A_o/A_t) = kt$$

where A_o and A_t are corresponding absorptions, measured at different illumination time, 'k' is rate of the reaction and 't'

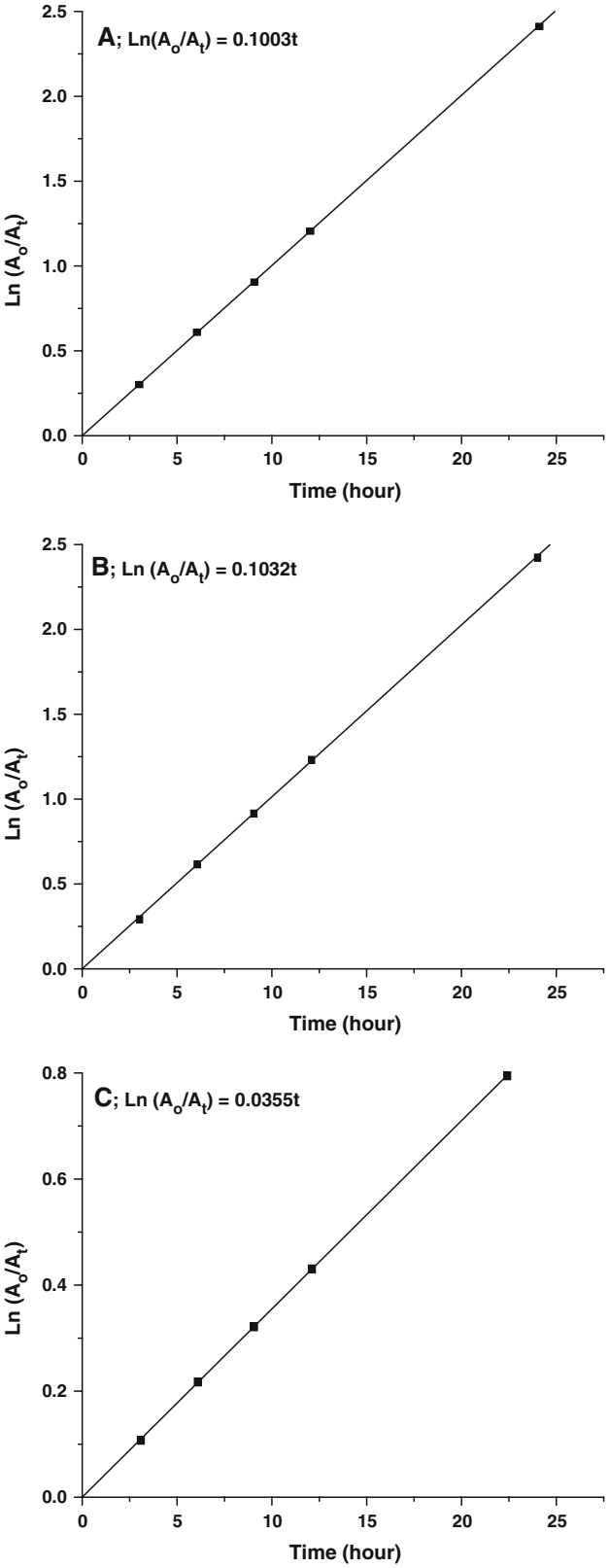

Fig. 9 Relationship between $\ln(A_o/A_t)$ and time during the decomposition of Procion Red MX-5B

is reaction time. The rate of the reaction k was calculated from all the three photodecomposition experiments by drawing a graph between $\ln(A_o/A_t)$ and time. Figure 9a–c shows the relation between $\ln(A_o/A_t)$ and time. Rate of the reaction k was obtained from the slope of these graphs and the as-obtained values are 0.1003, 0.1032, and 0.0355 h^{-1}, which, respectively, correspond to photodecomposition reaction with WO_3 rectangular slab, nanowire clusters and nanorod structures. Comparatively a high photodecomposition was noted from WO_3 nanowire cluster samples.

Conclusion

Self-assembled WO_3 nanostructures were synthesized with new structure-directing chemicals by using hydrothermal route and its structural, optical, and photodecomposition activity were studied. We have obtained different WO_3 morphologies like rectangular slab, nanowire clusters, and nanorods by introducing new structure-directing chemicals (ferrous ammonium sulfate, cobalt chloride) in this hydrothermal reaction. The possible growth mechanism of various shaped WO_3 nanostructures was also discussed. From optical absorption maxima, quantum confinement effect was realized for all the three morphologies. From photodecomposition experiment, a relatively high photodecomposition activity was observed from nanowire clusters sample due to their high absorption. Further study is under research to investigate the concentration-dependent morphologies and their role in photodecomposition.

Acknowledgments The author would like to thank Dr. K. Swaminathan, Professor and Head, Department of Microbial Biotechnology, Bharathiar University for his support in utilizing UV–Vis absorption spectrophotometer. One of the authors S. Rajagopal would like to thank Bharathiar University for awarding University Research Fellowship to carry out this work.

References

1. B. Cao, J. Chen, X. Tang, W. Zhou, J. Mater. Chem. **2323**, 19 (2009)
2. M. Miyauchi, Phys. Chem. Chem. Phys. **6258**, 10 (2008)
3. M. Hoping, C. Schildknecht, H. Gargouri, T. Riedl, M. Tilgner, H.H. Johannes, W. Kowalsky, Appl. Phys. Lett. **213306**, 92 (2008)
4. M. Sadakane, K. Sasaki, H. Kunioku, B. Ohtani, W. Ueda, R. Abe, Chem. Commun. 6552 (2008)
5. X. Cui, L. Guo, F. Cui, Q. He, J. Shi, J. Phys. Chem. C **4134**, 113 (2009)
6. K. Huang, Q. Pan, F. Yang, S. Ni, X. Wei, D. He, J. Phys. D: Appl. Phys. **155417**, 41 (2008)
7. S.R. Bathe, P.S. Patil, Smart Mater. Struct. **025004**, 18 (2009)
8. S.N. Alamri, Smart Mater. Struct. **025010**, 18 (2009)
9. Z. Luo, J. Yang, H. Cai, H. Li, X. Ren, J. Liu, X. Liang, Thin Solid Films **5541**, 516 (2008)
10. A. Mozalev, V. Khatko, C. Bittencourt, A.W. Hassel, G. Gorokh, E. Llobet, X. Correig, Chem. Mater. **6482**, 20 (2008)
11. Y. Zhang, Y. Chen, H. Liu, Y. Zhou, R. Li, M. Cai, X. Sun, J. Phys. Chem. C **1746**, 113 (2009)
12. A.A. Ashkarran, A. Irajizad, M.M. Ahadian, S.A.M. Ardakani, Nanotechnology **195709**, 19 (2008)
13. K.J. Lethy, D. Beena, V.P. Mahadevan Pillai, V. Ganesan, J. Appl. Phys. **033515**, 104 (2008)
14. Z. Gu, T. Zhai, B. Gao, X. Sheng, Y. Wang, H. Fu, Y. Ma, J. Yao, J. Phys. Chem. B **23829**, 110 (2006)
15. Z. Gu, Y. Ma, W. Yang, G. Zhang, J. Yao, Chem. Commun. 3597 (2005)
16. Z. Gu, H. Li, T. Zhai, W. Yang, Y. Xia, Y. Ma, J. Yao, J. Solid. State. Chem. **98**, 180 (2007)
17. X. Song, Y. Zhao, Y. Zheng, Mater. Lett. **3405**, 60 (2006)
18. S. Komaba, N. Kumagai, K. Kato, H. Yashiro, Solid State Ionics **193**, 135 (2000)
19. P. Delichere, P. Falaras, M. Froment, A.H. Goff, B. Agius, Thin Solid Films **35**, 161 (1988)
20. M.F. Daniel, B. Desbat, J.C. Lassegues, B. Gerand, M. Figlarz, J. Solid State Chem. **235**, 67 (1987)
21. O.Y. Khyzhun, J. Alloys Compd. **1**, 305 (2001)
22. K. Hong, M. Xie, R. Hu, H. Wu, Appl. Phys. Lett. **173121**, 90 (2007)
23. K. Lee, W.S. Seo, J.T. Park, J. Am. Chem. Soc. **3408**, 125 (2003)
24. M. Feng, A.L. Pan, H.R. Zhang, Z.A. Li, F. Liu, H.W. Liu, D.X. Shi, B.S. Zou, H.J. Gao, Appl. Phys. Lett. **141901**, 86 (2005)
25. S. Pal, C. Jacob, J. Mat. Sci. **5429**, 41 (2006)
26. C. Hu, J.C. Yu, Z. Hao, P.K. Wong, Appl. Catal. B: Environ. **47**, 42 (2003)